# Measurement and qualitative explanation of decay lengths of attractive and repulsive forces between natural and artificial atoms

Marco Weiss, Fabian Stilp, Max Reinhart, and Franz J. Giessibl*
*Institute of Experimental and Applied Physics, University of Regensburg, 93053 Regensburg, Germany*

(Received 24 July 2025; revised 9 October 2025; accepted 10 October 2025; published 13 November 2025)

Artificial atoms, such as quantum corrals, offer an excellent platform to study fundamental interactions between localized quantum states and nanoscale probes. We performed atomic force microscopy measurements inside square quantum corrals on Cu(111) using CO- and metal-terminated tips. Using chemically unreactive CO-terminated tips, repulsive Pauli forces can be probed, while metallic tips are attracted to the localized quantum states due to chemical bonding. We found distinct exponential decay constants of $(46 \pm 6)$ pm for the repulsive and $(66 \pm 5)$ pm for the attractive forces. Attractive and repulsive interactions between two natural atoms show significantly shorter decay lengths. While natural atoms feature states with a broad range of decay lengths, including very short ones from deeply bound states, quantum corrals are lacking such deeply bound and highly localized states, resulting in longer decay lengths. These results offer an alternate route to understanding and designing atomic-scale interactions in low-dimensional quantum structures and devices.

DOI: 10.1103/2bsk-8cvx

## I. INTRODUCTION

The ability to control and manipulate matter at the atomic scale is a fascinating aspect of modern nanoscience and nanotechnology. A landmark achievement was the development of atomic manipulation [1] using the scanning tunneling microscope (STM). Manipulating single atoms not only provides unprecedented visualization of surfaces [2], but also allows the construction of artificial quantum structures with dimensions all the way down to the nanometer scale. Atomic manipulation has proven to be remarkably versatile, allowing the exploration of fundamental quantum states in systems such as Dirac materials, including Lieb lattices [3,4] and artificial graphene [5], as well as in structures with interesting topological behavior [6–8], just to name a fraction of what has been studied previously. It has also been applied to practical challenges, such as manipulating and sensing the spin state of artificial atomic structures (e.g., Refs. [9–11]), logic operations [12,13], or pushing the limits of storing data at the atomic scale [14,15].

By arranging adsorbates with atomic precision, researchers also gained the ability to tailor the confinement of electrons within these structures [16–18]. Quantum corrals [19], formed by positioning atoms in a closed geometry on a surface, are a prime example. The closed geometry confines surface state electrons in the $x$ and $y$ plane (surface plane), leading to a set of resonant eigenstates inside the corral. By confining a fixed number of electrons in a small space such that a discretized energy spectrum is present, quantum corrals can be regarded as artificial atoms [20,21]. Since the original circular quantum corral, made from Fe adatoms on Cu(111), was introduced in 1993 [19], artificial atoms have been realized on a variety of more exotic surfaces, including semiconductors [22], Rashba surface alloys [23], proximity superconductors [17], and topological insulators [24]. These structures have become essential model systems, allowing researchers to explore fundamental quantum phenomena in designed environments using STM.

Atomic force microscopy (AFM) has emerged as a complementary technique to STM, offering the ability to probe surface properties with atomic spatial resolution and femtonewton force sensitivity. While STM exclusively probes the electronic behavior of quantum structures such as artificial atoms, AFM allows for direct investigation of the forces that are determined by the interaction between the confined electronic states and the probe tip, an aspect STM does not provide. Understanding these interactions is vital for potential applications in quantum technology, such as quantum sensing or quantum computing. Quantum sensors often rely on the interactions between the sensor and a probe (e.g., Refs. [25,26]). Such sensors are very sensitive to even weak interactions, and the performance of such devices depends greatly on the understanding of how probes (e.g., the AFM tip) interact with the quantum system (e.g., the quantum corral). Quantum computing, on the other hand, requires precise control over quantum states (qubits) (e.g., Refs. [27–31]). Any unwanted or poorly understood interaction can lead to errors and decoherence. Therefore, a fundamental understanding of the forces that act on confined electronic states in quantum structures is important for the development of more robust and reliable qubits and quantum sensing devices.

AFM studies by Stilp *et al.* [21] have demonstrated the ability to probe these tip-sample interactions within quantum corrals, revealing femtonewton-scale forces between the AFM tip and confined electronic states. Specifically, they observed a repulsive force when using a CO-terminated tip, attributed to Pauli repulsion, and an attractive force with a metal-terminated tip, suggesting the formation of a chemical

*Contact author: franz.giessibl@ur.de

 

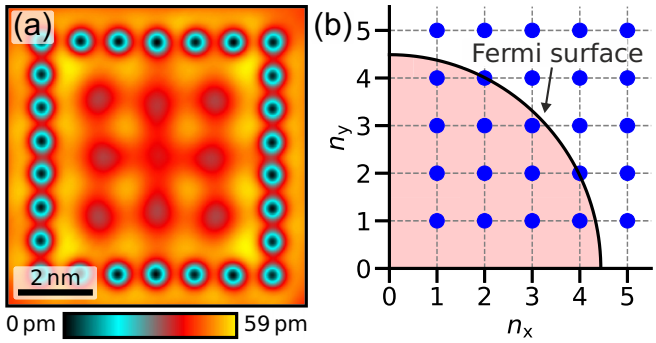


FIG. 1. (a) STM topography image of the square corral, consisting of 26 CO molecules, measured with a metal tip, a sample bias of 10 mV, and a tunneling current set point of 100 pA. The side lengths are 6.132 nm (horizontal) and 6.195 nm (vertical). CO molecules appear as dark dips. In the inner part of the corral, the charge density near the Fermi level can be seen as the checkerboard-like structure. (b) Model spectrum of the square shaped corral in (a) in $n$-space, characterized by the main quantum numbers $n_x$ and $n_y$. All states (blue markers) which lie in the red shaded region are below the Fermi level and are therefore occupied with electrons.

bond. Although this study established the sensitivity of AFM to these interactions, no detailed discussion of the decay characteristics was given.

In this work, we present an AFM study of the interactions between the confined electronic state within square-shaped quantum corrals on a Cu(111) substrate and AFM tips with CO and metal terminations. Our research offers a detailed analysis of the attractive and repulsive forces, revealing distinct decay lengths of 46 pm for repulsion and 66 pm for attraction. We further demonstrate that the measured force decays deviate form the conventional decay ratio found in the semiempirical Morse potential, where there is a factor of 2 between the attractive and repulsive decay lengths. Based on our data, we estimate an upper limit of 1.6 for this factor. Additionally, a comparison of the decay lengths measured in a quantum corral with those observed between two natural atoms reveals a significant difference: Natural atoms typically exhibit decay lengths that are significantly shorter than the ones measured in a quantum corral. This can be attributed to the presence of deeper bound states in natural atoms, which contribute to interactions with a short decay length. Conversely, the quantum corral system lacks such deeply bound and highly localized states, which in turn leads to the longer decay lengths observed. This comparison highlights principles critical to understanding both the decay characteristics of interactions between natural atoms and the design of low-dimensional quantum structures with tailored chemical reactivity.

## II. THE QUANTUM CORRAL

The quantum corral built for this work is square shaped and consists of 26 individually positioned CO molecules. An STM topography image is shown in Fig. 1(a). For details on the measurement conditions and experimental setup, see the Supplemental Material SM1 [32]. The side lengths of the quantum corral are 6.132 nm (horizontal) and 6.195 nm (vertical). Details about the exact adsorption sites of the CO molecules are provided in the Supplemental Material SM2 [32]. For the upper and lower corral walls, the intermolecular distance is 1022 pm, while the left and right walls have an intermolecular spacing of 885 pm.

A quantum corral on Cu(111) confines the quasi-free two-dimensional (2D) electron gas present on the surface (also called the Shockley surface state [40]), resulting in a set of resonant eigenstates [19]. To understand the behavior of the confined Shockley surface state within the quantum corral, a model description of a particle in a 2D box can be used. It was shown that an infinitely high potential well in the $x$ and $y$ plane (surface plane) captures the main properties of a quantum corral, including the spatial shape and energetic position of the resonant eigenstates [18,19,21]. In the $x$ and $y$ directions there are sinusoidal-shaped standing waves characterized by the quantum numbers $n_x$ and $n_y$. These quantum numbers determine the energy and shape of the confined electron wave functions $\Psi_{n_x,n_y}(x, y)$. For explanatory purposes, a modeled spectrum of the quantum corral in $n$-space is given in Fig. 1(b). Each marker represents a single corral state, which is characterized by its main quantum numbers $n_x$ and $n_y$. All corral states below the Fermi level [within the red-shaded region in Fig. 1(b)] are occupied with electrons. A more detailed discussion about the model description of the quantum corral is provided in the Supplemental Material SM3 [32].

Stilp *et al.* were the first to show the measured forces between the AFM tip and the Shockley surface state confined in a quantum corral scale with the total surface charge density $\sigma_{\text{tot.}}$ [21]. The total surface charge density is determined by which corral states lie below the Fermi energy $E_F$ and are therefore occupied by electrons: $\sigma_{\text{tot.}}(x, y) \propto \sum_{E_{n_x,n_y} \leqslant E_F} |\Psi_{n_x,n_y}(x, y)|^2$. Metal tips showed a stronger chemical attraction to regions with an increased total surface charge density, whereas CO-terminated tips are repelled from regions with an increased surface charge density. This repulsive force was attributed to Pauli repulsion [21].

The decay of the corral states toward the vacuum ($z > 0$) is not affected by the lateral confining structure (the walls) and is described by $\Psi_z(z) \propto \exp(-z/\lambda_S^\Psi)$ with $\lambda_S^\Psi$ being the decay constant of the sample wave functions. Calculations by Stilp *et al.* [21] showed that corral states decay with $\lambda_S^\Psi = 84$ pm toward the vacuum. Consequently, the corresponding electron density ($|\Psi|^2$) decays with a length of 42 pm.

## III. EXPERIMENTS AND MODEL DESCRIPTION

### A. Constant height AFM images and the total surface charge density

In Fig. 2(a) a constant height AFM image of the inner part of the quantum corral is provided, measured with a CO-terminated tip and a sample bias of $V_B = 0$ V. This image was taken at a tip-sample distance of 340 pm, defined by the core-core distance of the frontmost oxygen atom and the copper surface layer [41]. The measurement signal $\Delta f$ is proportional to the force gradient between tip and sample [42]. At such a small tip-sample separation, the Cu surface atoms are visible as small attractive (dark) features [35,43]. Overlaid with this copper grid, wider features can be recognized. This

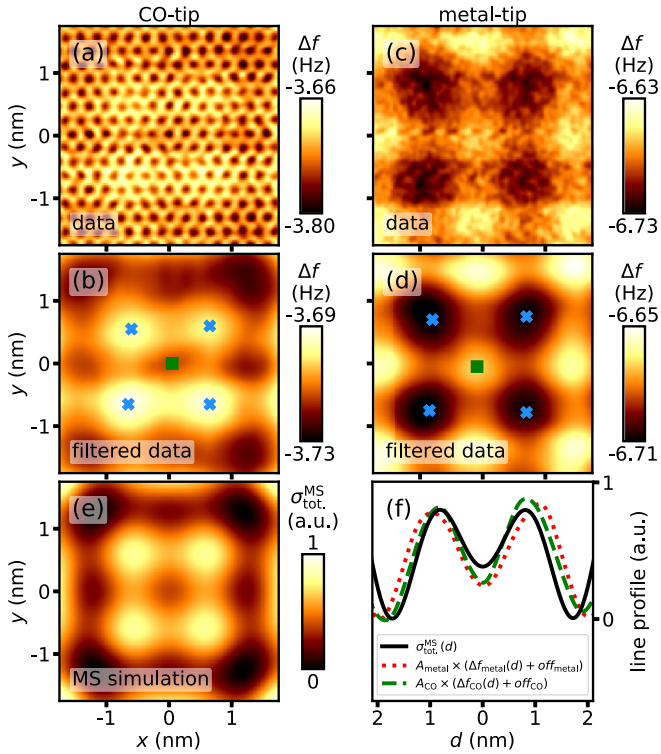


FIG. 2. (a) Frequency shift ($\Delta f$) image measured with a CO tip in constant height showing the Cu surface atoms as small dark dips. The confined surface state is visible as the superimposed four bright spots around the center surrounded by eight light-dark dips. (b) Gaussian low-pass filtered version of (a) to remove the Cu grid [21,32]. (c) Frequency shift image measured with a metal tip in constant height. The confined surface state is visible as four dark dips around the center surrounded by eight bright spots. (d) Slightly Gaussian low-pass filtered version of (c). (e) Multiple scattering simulation of the total surface charge density $\sigma_{\text{tot}}^{\text{MS}}$. The appearance of (b) and (d) only differs by a minus sign, showing that local accumulations of the surface charge density lead to repulsion when measured with a CO tip [bright regions in (b)], and attraction [dark regions in (d)] when measured with a metal tip. (f) Average of the two diagonal line profiles of the CO tip AFM image from (b), shown as the green dashed line. In this plot $d$ is defined as the distance from the center of the corral. For qualitative comparison, an offset of $\text{off}_{\text{CO}} = 3.73$ Hz was added and the result multiplied by an amplitude factor of $A_{\text{CO}} = 31\ \frac{\text{a.u.}}{\text{Hz}}$: $A_{\text{CO}} \times (\Delta f_{\text{CO}} + \text{off}_{\text{CO}})$. The red dotted line shows the corresponding profile from the metal tip AFM image in (d), scaled by using $\text{off}_{\text{metal}} = 6.65$ Hz and $A_{\text{metal}} = -14.7\ \frac{\text{a.u.}}{\text{Hz}}$. The black line represents the simulated profile of (e). This comparison illustrates that both AFM images reflect the total surface charge density $\sigma_{\text{tot}}^{\text{MS}}$.

additional signal stems from the confined surface state and consists of four bright spots around the center of the image surrounded by eight light-dark dips. Applying a Gaussian low-pass filter (see SM4 [32] for more details) to Fig. 2(a) suppresses the spatially high-frequency atomic surface lattice signal and shows the confined surface state more clearly [see Fig. 2(b)].

When AFM measurements are performed with a metal tip [see Figs. 2(c) and 2(d)], the opposite behavior is found. Metal tips interact attractively with corral states, resulting in an increased attraction over regions with a high $\sigma_{\text{tot.}}$ (dark areas).

To simulate the total surface charge density, multiple scattering (MS) simulations are employed. The MS formalism developed by Heller *et al.* [44] is based on an $s$-wave scattering approach and is an established method to simulate the electronic properties of a quantum corral. It has been shown that the best agreement between experiment and MS simulation can be achieved when the $\delta$-peak-shaped scattering potentials are provided with a strong absorbing channel [44], which is called the "black-dot" limit. Our simulations showed that the confined surface state electrons exhibit a slightly higher effective mass $m^*_{\text{e,conf.}}$ than the free surface state electrons $m^*_{\text{e,free}}$. The best agreement between simulation and measurement was found for $m^*_{\text{e,conf.}} = 0.45 \times m_{\text{e}}$, while the effective mass of the free Shockley surface state is $m^*_{\text{e,free}} = (0.405 \pm 0.025) \times m_{\text{e}}$ (e.g., Refs. [45–50]). The slight increase in effective mass of confined electrons is a known phenomenon that has also been observed, for example, in semiconductor quantum dots [51]. Furthermore, Freeney *et al.* [52] also simulated square-shaped quantum corrals on Cu(111) with a muffin tin model and found effective masses of $0.48 \times m_{\text{e}}$ and $0.46 \times m_{\text{e}}$, which is in good agreement with the effective mass we found. The effective mass was determined to ensure a correct simulation, and consistency between simulation and experiment, but it is not central to our analysis and will not be discussed further. Additional details on the MS simulations are given in the Supplemental Material SM5 [32].

The simulated total surface charge density $\sigma_{\text{tot.}}^{\text{MS}}$ is shown in Fig. 2(e). In this image, bright regions correspond to a high total surface charge density, while dark regions correspond to a low total surface charge density. Comparison of Figs. 2(b) and 2(e) again makes it clear that AFM measurements, conducted with a CO-terminated tip, are sensitive to the total surface charge density, where an increased total surface charge density [bright regions in Fig. 2(e)] results in an increased repulsive force [bright areas in Fig. 2(b)]. The opposite behavior can be found when comparing the metal tip AFM image [Figs. 2(c) and (d)] with the simulation of the total surface charge density [Fig. 2(e)]. An increased total surface charge density [bright regions in Fig. 2(e)] results in a more attractive force [dark in Fig. 2(d)]. Regions with a minimum of total surface charge density [dark in Fig. 2(e)] will result in a minimal attractive force, which appears bright in AFM images [see bright regions in Fig. 2(d)]. In Fig. 2(f) the average line profiles along the two diagonals of the respective images are shown. To show qualitative agreement, an offset was added to all measured line profiles and then multiplied by an amplitude factor. Details are provided in the caption of Fig. 2(d). Please note that the line profile of the metal tip AFM image (red dotted line) was multiplied with a negative amplitude factor, effectively inverting the profile line.

It is worth noting that the maxima of the profile lines in Fig. 2(d) are further apart for the metal tip measurement than for the CO tip measurement. For the metal tip the maxima are separated by 2 nm, while for the CO tip they are separated by 1.7 nm. Approaching an AFM tip close to the surface can shift the energy of the corral states [21]. It was shown that CO tips slightly raise the energy of corral states, leading to a small depopulation of corral states near the Fermi energy. In

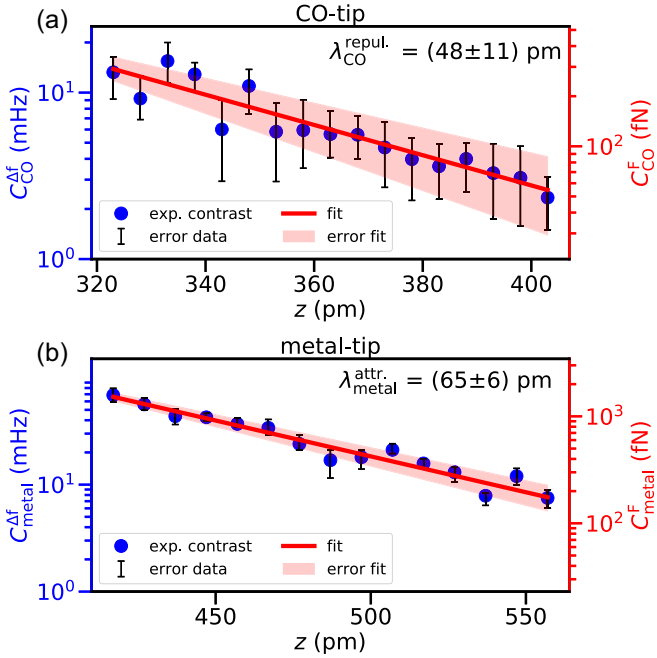


FIG. 3. (a) Contrast in $\Delta f$, measured with a CO tip, as a function of vertical distance $z$ showing an exponential behavior with a decay length of $\lambda_{CO}^{repul.} = (48 \pm 12)$ pm. The contrast is defined as the difference between the average of the four innermost maxima and the central minimum. (b) Contrast in $\Delta f$, measured with a metal tip, with a decay length of $\lambda_{metal}^{attr.} = (64 \pm 7)$ pm. The contrast is defined as the difference between the central maximum and the average of the four innermost minima. The definition of the error bars of the data points is described in the Supplemental Material SM7 [32]. In both cases the $\Delta f$ contrast was fitted with an exponential decay function. The fits are displayed as full red lines and can be associated to a force contrast (right axis). The red shaded region gives the error of the fit, which is two times the standard deviation.

contrast, metal tips lower the state energies, slightly increasing the electron occupation. These tip-induced shifts affect the total surface charge density and can explain the subtle differences between the CO and metal tip profile lines. This confirms the interpretation of the tip-induced energy shifts shown by Stilp *et al.* [21] in circular quantum corrals. A more detailed discussion is provided in the Supplemental Material SM6 [32]. Multiple scattering simulations do not account for such a tip-induced energy shift. The calculated $\sigma_{tot}^{MS}$ might also deviate moderately from the measurements as -440 meV for the band edge of the Shockley surface state was used, a value that varies slightly in literature.

### B. Decay lengths of the attractive and repulsive forces

Recording constant height AFM images at different tip-sample separations additionally provides insight into the distance dependence of the interaction between the tip and the corral states. Figure 3 shows the contrast evolution of the frequency shift $C^{\Delta f}$ as a function of the tip-sample distance $z$. Each $C^{\Delta f}$ value in Fig. 3 was calculated from one constant height AFM image. The contrast is defined by the absolute difference between the four innermost extrema, marked by blue crosses, and the center, marked by the green square [see Figs. 2(b) and 2(d)]. More details about the calculation of the contrast are provided in the Supplemental Material SM7 [32].

TABLE I. AFM force contrast decay lengths measured with a CO and a metal tip. Corral 1 was measured using a monoatomic metal tip, followed by measurements with a CO-terminated tip (same metal tip but equipped with a CO at the apex). Corral 2, built after several preparation cycles on the same copper crystal, was measured using a different mesoscopic tip configuration [54]. To verify the reproducibility of the decay lengths, measurements with the CO tip were repeated twice. Corral 3, which featured denser walls, was measured using the same CO and metal tip as for corral 1.

| | $\lambda_{CO}^{repul.}$ (pm) | $\lambda_{metal}^{attr.}$ (pm) |
|---|---|---|
| Corral 1 (Fig. 1–3) | 48±11 | 65±6 |
| Corral 2 (SM8 [32]) | 40±13<br>39±14 | 67±8 |
| Denser corral (Fig. 4) | 51±9 | 68±13 |
| Average | 46±6 | 66±5 |

For both tip configurations (CO and metal tip), the contrast decays exponentially with $z$, resulting in decay lengths of $\lambda_{CO}^{repul.} = (48 \pm 11)$ pm and $\lambda_{metal}^{attr.} = (65 \pm 6)$ pm. The force contrast $C^F$ follows from Eq. (8) in Ref. [53]: $C_{CO}^F(z) = 291\ \text{fN} \times \exp[-(z - 323\ \text{pm})/\lambda_{CO}^{repul.}]$ for the CO tip measurements and $C_{metal}^F(z) = 1522\ \text{fN} \times \exp[-(z - 417\ \text{pm})/\lambda_{metal}^{attr.}]$ for the metal tip measurements. This means that for the smallest tip-sample separations (323 pm for CO tip and 417 pm for metal tip) force contrasts of 291 and 1522 fN were measured. The respective force contrasts are shown as full red lines in Fig. 3. For reproducibility, additional measurements were made using different CO and metal tips in a separate corral [54]. The corresponding analysis is provided in the Supplemental Material SM8 [32] and is summarized in Table I. It is evident that the obtained decay lengths are consistent with the measurement accuracy. This demonstrates that the decay lengths are independent of the mesoscopic tip geometry and the environment of the quantum corral.

Because the interaction between the tip and the corral states decays exponentially on a length scale of only a few tens of picometers, the dominant contribution arises from the frontmost atom of the tip apex. In the case of a monoatomic metal tip, atoms in the second layer are located approximately 200 pm farther from the surface. With a decay length of 66 pm, their contribution to the force is therefore only about 5% that of the apex atom and can safely be neglected. Consequently, the macroscopic geometry of the tip barely influences the measured interaction.

Recently, it was demonstrated that the eigenstates of quantum corrals are influenced by the wall density. Higher wall densities cause a slight shift in the energies of the corral states toward higher values and also extend the lifetimes of these states [18]. However, the decay of the corral states into the vacuum should not be affected by the wall density. To show this, AFM measurements were also performed in a corral with twice the wall density compared to the one presented in Fig. 1(a). The decay lengths of the denser quantum corral are

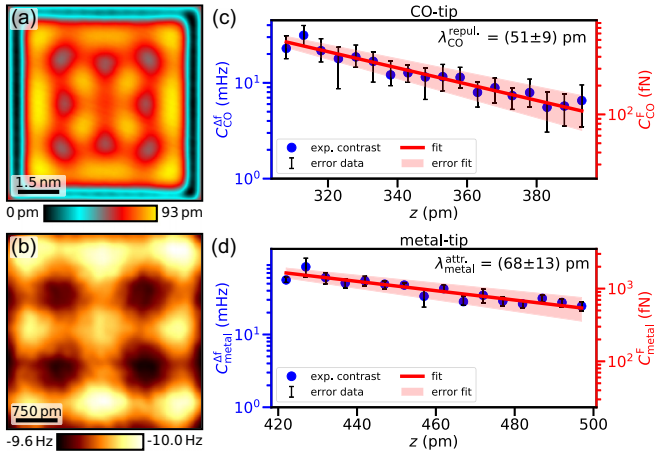


FIG. 4. (a) STM topography image of the denser square corral measured with a metal tip, a sample bias of −10 mV, and a tunneling current set point of 100 pA. This corral also has side lengths of 6.132 and 6.195 nm but consists of 52 CO molecules. The image has a size of 7 by 7 nm. (b) Frequency shift image measured with a metal tip in constant height. This measurement was taken inside the quantum corral and has a size of 3.8 by 3.8 nm. (c) and (d) Contrast in $\Delta f$ and $F$, measured with a CO and a metal tip, as a function of vertical distance $z$ showing an exponential behavior with decay lengths of $\lambda_{CO}^{repul.} = (51 \pm 9)$ pm and $\lambda_{metal}^{attr.} = (68 \pm 13)$ pm.

listed in Table I and the corresponding analysis is shown in Fig. 4.

As shown in Table I and Fig. 4, the measured decay lengths remain unchanged within the measurement accuracy, regardless of the mesoscopic tip configuration or the wall density of the corral. This demonstrates a clear relationship between the decay lengths of the interaction of the confined Shockley surface state with a metal and a CO tip (attractive and repulsive):

$$\lambda_{metal}^{attr.} = (1.4 \pm 0.2) \times \lambda_{CO}^{repul.}. \tag{1}$$

Equation (1) shows that in the case of the corral, the decay lengths of Pauli repulsion and chemical bond differ by a factor of 1.4. This result shows a clear difference between the decay lengths of the attractive and repulsive interactions with a confined Shockley surface state.

As discussed earlier in Sec. III A and SM6 [32], the close proximity of the AFM tip can slightly shift the center energy of the corral states. This alters their occupation and, consequently, the total surface charge density [see the difference between attractive and repulsive profile lines in Fig. 2(f)]. In general, such changes could influence the distance dependence of the $\Delta f$ contrast. Corral states in denser structures have longer lifetimes and therefore narrower energy distributions [18], making their total surface charge densities more sensitive to tip-induced shifts. However, since both dense and less-dense corrals yield the same decay length (see Table I), we conclude that the influence of this effect on the measured decay length is negligible.

It is well known that CO at the apex of an AFM tip is a rather flexible termination that can bend laterally during scanning. When imaging molecules on surfaces, such CO bending can even enhance spatial resolution. From the measured force contrast with a CO-terminated tip, one can estimate that the corresponding potential energy corrugation in a quantum corral is very shallow (90 μeV). The resulting lateral forces on the CO lead to a negligible lateral deflection of approximately 60 fm. We therefore conclude that CO bending does not affect the measured decay lengths. Further details on this estimation are provided in the Supplemental Material [32].

### C. Model description of the attractive and repulsive forces

The extracted decay length of the CO tip measurement is greater than the decay length of the surface charge density ($\lambda_S^{\Psi}/2 = \lambda_S^{\rho} = 42$ pm). This can be understood with a commonly used model description of Pauli repulsion, which is given by the overlap integral of the total charge densities of the tip $\rho_{CO\ tip}$ and sample $\rho_{sample}$:

$$F_{Pauli,z} \propto \frac{\partial}{\partial z} \int [\rho_{CO\ tip}(\vec{r}) \rho_{sample}(\vec{r})]^{\alpha} \mathrm{d}\vec{r}, \tag{2}$$

with $\alpha \approx 1$ (e.g., Refs. [55–58]). From this relationship, it becomes evident that the measured force contrast conducted with a CO tip in quantum corrals depends not only on the decay length of the total charge density of the sample but also on that of the tip. As an estimate, the charge density at the apex of the CO tip can be modeled as an $s$-wave-like distribution (i.e., Slater-type functions for large distances from the atomic nucleus). With an effective nuclear charge $Z_{eff} \approx 4.5$ of the valence electrons of oxygen [59], the charge density of the front most part of the CO tip approximately decays with 12 pm. With this the model description of Pauli repulsion gives a decay length of the force of $\lambda_{Pauli,z}^{model} = 43$ pm with $\alpha = 1$ which is slightly larger than the charge density decay of the Shockley surface state (see Supplemental Material SM9.1 for more details [32]). The modeled decay length also lies within the measured error window of $46 \pm 6$ pm.

Despite the good agreement, we found three possible reasons why the modeled decay length of Pauli repulsion is slightly shorter than the measured length. None of those is the $s$-wave approximation of the flat corral states, as this is justified in SM9.5 [32].

One possibility lies in the fact that the Shockley surface state decay length was calculated using the known work function of Cu(111). The close proximity of the AFM tip can locally alter the potential landscape of the surface, effectively modifying the work function [60,61]. Such a perturbation could lead to a longer decay length than expected from ideal, unperturbed surface parameters. An effective work function of $\Phi_{eff.}^{CO\ tip} \approx 4.5$ eV is needed to closely match the measured decay lengths.

Another contributing factor may be the scaling exponent $\alpha$, which appears in the density-overlap-based model of Pauli repulsion [55,57]. Although set to unity in this work for clarity and consistency, it was shown that $\alpha$ can vary depending on the nature of the interacting systems. Values slightly above 1 have been reported for molecular systems [57], while interactions between single natural atoms often yield values slightly below 1 [55]. A value of $\alpha = 0.92$ results in a modeled decay length that closely matches the measured length. This suggests that modest deviations from the idealized scaling

behavior may be intrinsic to the corral system and should be taken into account in future refinements of the model.

A third possibility could result from an influence of long-range attractive interaction between CO tip and corral states. Stilp *et al.* [21] showed that the attractive electrostatic interactions between the tip and the corral states are small and therefore can be neglected. Due to the formation of a compensation layer of electron depletion below the corral state with the same spatial distribution and opposite sign, the resulting electrostatic forces are strongly reduced. Furthermore, the decay length of the remaining electrostatic interaction is on the order of several hundred picometers. When considering the contrast in $\Delta f$, any long-range contributions, including also other forces such as van der Waals attraction, are suppressed, leaving only the short-ranged Pauli repulsion between the tip and the corral state.

The distance dependence of chemical bonding is often approximated by the overlap of wave functions (e.g., Refs. [61–64]): $F_{\mathrm{chem},z} \propto \frac{\partial}{\partial z} \int \Psi_{\mathrm{tip}}(\vec{r})\Psi_{\mathrm{sample}}(\vec{r})\mathrm{d}\vec{r}$. In the relevant energy regime around the Fermi level, metallic tips are predominantly characterized by *s*-orbitals [65] with an estimated decay length of ≈84 pm [66,67]. This simplified model predicts a chemical force decay length of 125 pm (see Supplemental Material SM9.2 for details [32]).

With this model description of the distance dependence of a chemical bond, the key difference between Pauli repulsion and chemical attraction is that the former depends on the absolute square of the wave functions ($\rho \propto |\Psi|^2$), while the latter depends on the wave function itself ($\Psi$). Because the charge densities of tip and sample decay as $|\Psi|^2$, the decay length of Pauli repulsion is inherently shorter than that of the chemical attraction. This trend is also reflected in our measurements, where Pauli repulsion results in a shorter decay length (CO tip, 46 pm) than chemical bonding (metal tip, 66 pm).

It is important to note that the chosen description of the chemical force between the metal tip and corral states is a simplified model. Although it qualitatively explains the observed difference in decay lengths, it results in a decay length twice as long as the measured one. A more sophisticated approach, such as a linear combination of atomic orbitals (LCAO) model, would inherently incorporate orbital overlap effects in a more detailed manner. However, the development of a complete LCAO-based description goes beyond the scope and purpose of this work.

The commonly used semiempirical Morse potential [68] provides a useful and intuitive model to describe the potential energy of diatomic molecules. It consists of two summed exponential functions, one describing the repulsive interaction (prominent for small separations) and one describing the attractive interaction (prominent for large separations). The Morse potential has been widely applied in various fields of science, ranging from the description of catalytic processes on surfaces to the simulation of dynamics in biological systems or gases [69]. Given this broad applicability, it also serves as a meaningful reference for AFM-based force analysis.

In the original Morse formulation, the attractive decay length is twice as long as the repulsive one, meaning $\mu = \lambda^{\mathrm{Morse}}_{\mathrm{attr.}}/\lambda^{\mathrm{Morse}}_{\mathrm{repul.}} = 2$. However, this ratio cannot be applied to the measurements presented here. Our data, recorded with a metal tip, clearly lie in the attractive regime which corresponds to the right side of the potential minimum. Attempting to access the repulsive regime was not feasible, as the strong forces between tip and sample caused tip deformations or even dropping tip material inside the corral. Therefore, the metal tip measurements were limited to the attractive tail of the interaction, and fitting a full Morse potential was not possible.

Instead, we approximated the interaction by fitting a single exponential function to the attractive side (see Figs. 3 and 4), which yields a decay length of 66 pm. However, fitting one side of a Morse-like potential with a single exponential function introduces a systematic overestimation. The steep repulsive term slightly distorts the shape of the attractive tail, which is not captured in such a simplified fit. A mathematical analysis (see SM10 [32]) shows that the fitted decay length $\lambda^{\mathrm{attr.}}_{\mathrm{metal}}$ is always greater than or equal to the true attractive decay length: $\lambda^{\mathrm{attr.}}_{\mathrm{metal}} \geqslant \lambda^{\mathrm{attr.}}_{\mathrm{real}}$. This implies that $\lambda^{\mathrm{attr.}}_{\mathrm{real}} \leqslant 66$ pm. If the original Morse ratio $\mu = 2$ is applied, this would suggest a decay length of the Pauli repulsion of $\lambda^{\mathrm{repul.}}_{\mathrm{real}} \leqslant 33$ pm. As shown for the CO tip measurements, Pauli repulsion in the corral is well described by the overlap integral of electron densities [see Eq. (2)], and the decay length of the surface state charge density $\lambda^{\rho}_{\mathrm{S}} = 42$ pm can be regarded as a lower bound for the repulsive decay length for the corral system (see SM9.4 [32]). This directly excludes the Morse factor of 2. Taking the measured attractive decay length as an upper limit, the maximum possible ratio is $\mu_{\mathrm{max}} = 66\,\mathrm{pm}/42\,\mathrm{pm} = 1.6$. While this does not contradict the general concept of the Morse potential, it shows that the specific decay ratio assumed in its original form is not applicable to the experimental conditions in this study.

A rough estimate of the repulsive decay length of the metal tip can be obtained by applying the same model used for the CO tip [electron density overlap in Eq. (2)]. While the repulsive regime could not be accessed directly in the experiment, this method yields a hypothetical decay length of approximately 52 pm (see SM9.3 for further details [32]). Taking this value as the relevant repulsive decay length, the upper bound of the decay length ratio reduces to $\mu_{\mathrm{max}} = 66\,\mathrm{pm}/52\,\mathrm{pm} = 1.3$. This defines an even stricter upper bound for the decay length ratio, further supporting that the original Morse ratio of 2 is incompatible for the quantum corral system.

### D. Comparison of an artificial atom to a natural atom

To better understand the measured decay lengths of tip-corral interactions, it is instructive to compare them with those observed in interactions between natural atoms. Similar to the artificial atom case, natural systems also show that chemical bonding generally decays slower than Pauli repulsion. However, the absolute decay lengths observed in natural atom-atom interactions are shorter than those found in the corral system.

For chemical bonding, Ternes *et al.* [61] reported decay lengths around 40 pm for interactions between a metal tip and individual Cu and Pt adatoms on Cu(111). Rubio-Bollinger *et al.* [70] found similar values for metallic adhesion between gold atoms in atomic junctions, with decay lengths of approximately 45 pm. In contrast, the attractive interaction measured in this work between a metal-terminated AFM tip and the corral states shows a much longer decay length of 66 pm.

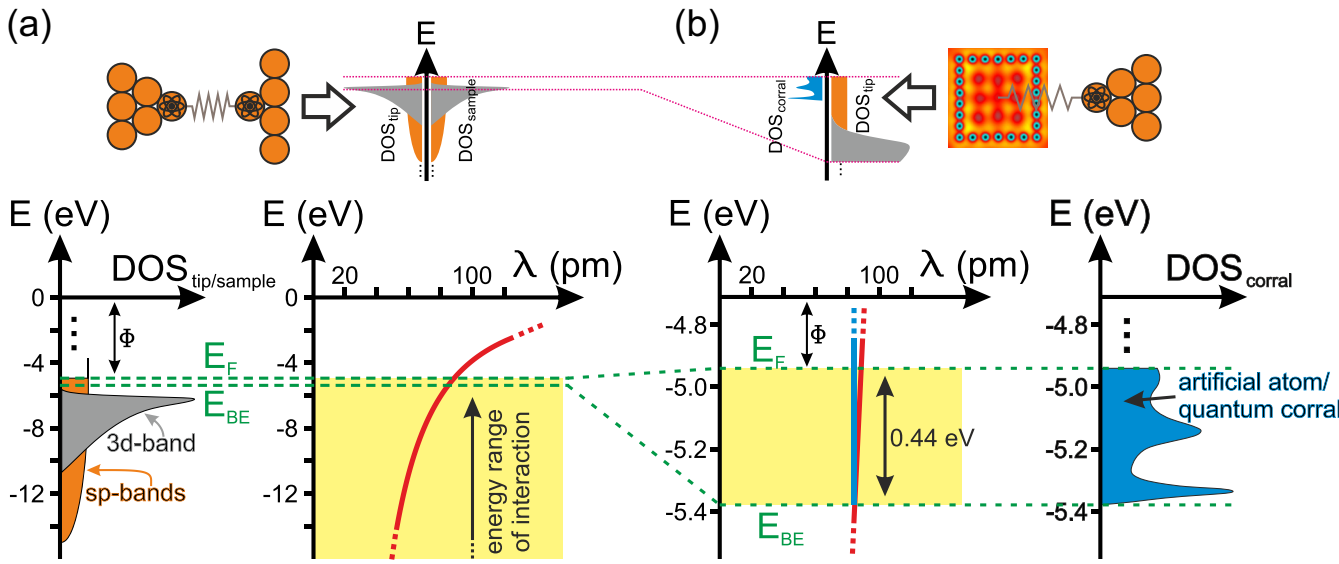


FIG. 5. Qualitative sketch of the electronic states involved in tip-sample interactions. (a) Bottom left: Schematic density of states (DOS) for a natural atom at the AFM tip apex and a natural adatom on a surface. For illustrative purposes, both DOS profiles (for tip and sample) are assumed to be identical. Tip and sample exhibit broad *sp*- and *d* bands. Lower-lying bands are not shown. $E_F$ is the Fermi energy, which is $\Phi = 4.94$ eV below zero energy, and $E_{BE}$ gives the band edge of the Shockley surface state. Bottom right: Approximated decay length $\lambda$ of electronic states in a natural atom configuration as a function of energy, following a $\lambda \propto 1/\sqrt{-E}$ dependence (see main text). (b) Electronic interaction between a natural atom and an artificial atom (quantum corral). The relevant energy range for interaction is defined by $E_{BE}$ and $E_F$. Within this narrow energy window the tip-side decay lengths vary only slightly (between 84 and 87 pm), while the decay length of the corral states remains constant at 84 pm (see graph at the bottom left side). Bottom right: Local density of states in the center of the corral (blue), extracted from a $dI/dV$ spectrum (see SM5 [32]). Top left: Comparison of the DOS profiles of tip and quantum corral. The DOS profile of the tip is a zoomed-in version of the natural atom profiles shown in (a). Averaged over the energy range of interaction, the natural-natural atom interaction has a shorter decay length than the natural-artificial atom interaction.

A comparable trend holds for Pauli repulsion. Measurements with CO-terminated tips on $CaF_2$ yielded repulsive decay lengths of 27 pm [58], and atomic scattering experiments report values around 28 pm across a range of various atomic species [71–76]. In contrast, the CO tip measurement over the quantum corral yields a repulsive decay length of 46 pm.

A likely explanation for this consistent difference lies in the nature and energy range of the electronic states involved in the interaction. Natural atoms have an energetically wide-spread distribution of electronic states, extending from the Fermi level down to deep-lying core levels. These states span several electron volts below $E_F$ and include orbitals that are highly localized in space. For instance, in Cu(111), the *sp* bands begin about 10 eV below the Fermi level and are energetically broad. The 3*d* band starts around 5 eV below $E_F$ and is nearly fully occupied. This is sketched on the lower left side of Fig. 5(a).

The energetic dependence of the decay length of states can be roughly approximated with an electronic state in a one-dimensional box. With the energy $E$ relative to the vacuum level (=0) the exponential decay length is given by $\lambda = \hbar/\sqrt{-2m_e E}$. For example, the 1*s* core level of copper, with a binding energy of roughly 9000 eV [77], has an approximated decay length of 2 pm. With an atomic spacing of 255 pm in bulk copper, such deeply bound orbitals barely overlap, and thus can be considered to not form bands. In contrast, decay lengths at the onset of the Shockley surface state (440 meV below $E_F$) are 84 pm. The energy dependence of the approximated decay lengths is shown on the lower right side of Fig. 5(a).

The total chemical interaction between two natural atoms is governed by contributions from many orbitals across a wide energy range. Long-ranging orbitals near the Fermi level decay slowly and begin to overlap at relatively large distances. As atoms come closer, deeper, more localized orbitals start to contribute, resulting in a faster increase in force. The full interaction can thus be seen as a combination of many orbital overlaps, each with its own distance dependence. This combined interaction decays faster than the Fermi-level component alone, which explains why experimental decay lengths for natural atoms are often significantly shorter than those of the highest-lying states. This is also the reason for the excellent spatial resolution of AFM [36].

The situation in the artificial atom (quantum corral) is different. The occupied electronic states of the corral lie within a narrow energy range of 440 meV below the Fermi level, as illustrated on the lower right side of Fig. 5(b). For the quantum corral there are no deeply bound and spatially highly localized states contributing to the interaction. Because of the 2D nature of the corral states, the decay lengths of all corral states are 84 pm. Within the narrow energy range of the occupied corral states, the approximated energy-dependent decay lengths of electronic states of natural atoms vary only slightly (from 84 to 87 pm). This is depicted on the lower left side of Fig. 5(b). The interaction is therefore governed solely by

slowly decaying states, resulting in longer decay lengths for both repulsive and attractive interactions compared to natural atom-atom systems.

That bonding in natural systems often involves deeper-lying states is also supported by several examples from literature. The 3*d* band of noble metals is known to play a critical role in the adsorption of CO, O, and $CO_2$ on copper clusters [78], as well as on transition metals like Cu, Ag, and Au [79]. This band is centered several electron volts below the Fermi level. In other cases, even fully filled semicore orbitals were shown to participate in bonding. For instance, the existence of $HgF_4$ is explained by bonding contributions from Hg's filled *d* orbitals [80], and $CsF_5$ has been predicted to form with bonding contributions from fully filled *p* orbitals [81]. Another example is the uranyl ion $UO_2^{2+}$, where the main bonding orbitals are 5*f* and 6*d*, but at short bond lengths, even the filled 6*p* semicore orbitals hybridize and contribute to the interaction [82–84]. It was further shown that also in solids, deeper-lying atomic orbitals participate in bonding [85]. These examples underline that bonding in natural systems can involve orbitals located well below the Fermi level, further supporting the conclusion that the effective decay length in such systems can be shortened by the participation of fast-decaying, deep-lying states.

## IV. SUMMARY AND OUTLOOK

### A. Summary

We performed constant-height AFM measurements with CO- and metal-terminated tips within a square-shaped quantum corral on Cu(111). Multiple scattering simulations supported the observation of previous studies [21] that the forces measured with AFM in quantum corrals scale with the total electron density. CO-terminated tips interact repulsively with the confined surface state, while metal-terminated tips interact attractively. We further found that the forces measured with CO- and metal-terminated tips decay exponentially with different decay lengths. The construction of a quantum corral with the same geometry but a denser wall confirmed that the decay lengths are independent of the corral wall and the mesoscopic tip shape. The repulsive interaction (CO tip) exhibited a decay length of $\lambda_{\mathrm{CO}}^{\mathrm{repul.}} = (46 \pm 6)$ pm, while the attractive interaction (metal tip) showed a decay length of $\lambda_{\mathrm{metal}}^{\mathrm{attr.}} = (66 \pm 5)$ pm. These decay lengths differ by a factor of $1.4 \pm 0.2$.

Modeling the repulsive interaction between a CO tip and the quantum corral states using an established model for Pauli repulsion (electron density overlap integral) yielded a modeled decay length of $\lambda_{\mathrm{model}}^{\mathrm{repul.}} = 43$ pm. Modeling the chemical attraction between a metal tip and the corral states using a wave function overlap integral showed the same trend as the measurements ($\lambda_{\mathrm{metal}}^{\mathrm{attr.}} > \lambda_{\mathrm{CO}}^{\mathrm{repul.}}$), but resulted in a too-long decay length.

Due to experimental constraints, a full Morse potential could not be fitted to the metal tip measurements. Instead, a single exponential was used to fit the attractive side, introducing a systematic overestimation of the attractive decay length ($\lambda_{\mathrm{metal}}^{\mathrm{attr.}} \geqslant \lambda_{\mathrm{real}}^{\mathrm{attr.}}$). Analysis showed that the original Morse potential's decay ratio of attractive to repulsive forces ($\mu = \lambda_{\mathrm{attr.}}^{\mathrm{Morse}}/\lambda_{\mathrm{repul.}}^{\mathrm{Morse}} = 2$) is not applicable to the corral system. Instead, the maximum possible ratio was found to be $\mu_{\max} = 1.6$. This demonstrates that the specific decay ratio assumed by Morse is not applicable to the experimental conditions of the quantum corral.

A comparison between natural and artificial atoms further reveals that the decay lengths of both attractive and repulsive interactions are significantly longer in the quantum corral system. This is attributed to the narrow energy window of occupied corral states near the Fermi level, which lack contributions from short-ranged, deep-lying orbitals. In contrast, natural atoms involve a broad spectrum of electronic states, including rapidly decaying orbitals far below $E_{\mathrm{F}}$, leading to a shorter effective decay length.

### B. Outlook

In their AFM study of circular quantum corrals, Stilp *et al.* were the first to reveal that confined surface states can establish chemical interactions with a metallic AFM tip, and they discovered attractive decay lengths of 50 and 56 pm [21]. The discrepancy in decay lengths between our results (square-shaped quantum corral, 66 pm) and their circular corral points to the possibility that the corral geometry influences the decay length and strength of chemical interactions. Further investigation of this relationship may show how the corral wave functions can be shaped to tailor the chemical reactivity of confined Shockley surface states.

Artificial nanostructures further offer an intriguing framework for investigating new electrical and chemical capabilities, going beyond single quantum corrals. Sierda *et al.* [22] developed a method for simulating the electronic structure of molecules using small, coupled quantum corrals on InSb. Building on this, it would be interesting to see if these simulated molecules have a similar chemical reactivity compared to their natural counterparts.

The emerging field of designer electronic structures has already produced fascinating systems with unique properties, such as Lieb lattices and artificial graphene [3–5] with Dirac cones, or SSH chains and kagome lattices with interesting topological behavior [6,7]. There, the natural questions arise: What bonding characteristics do these exotic electronic states exhibit, and do a CO and a metal tip interact with these exotic states in a manner similar to that with a single quantum corral?

Moreover, quantum corrals were already built on nontraditional materials such as topological insulators [24], proximity superconductors [17], semiconductors [22], graphene [86], or Rashba surface alloys [23]. Within these frameworks, investigating the chemical bonding interactions of corral states to a probe tip may present a promising direction for future exploration. All of these potentially interesting artificial nanostructures can also be measured with different tip terminations. Established tip terminations include, among others, Xe [87,88], copper oxide [89,90], or even magnetic molecules such as nickelocene [91]. Performing experiments similar to those presented here with different tip terminations could drastically increase the understanding of the nature of chemical bonds in a controlled environment with tunable chemical reactivity. Also, spin-polarized tips [92,93] could be used to investigate bonding properties of corral states on surfaces

where magnetism plays a crucial role (e.g., corrals on topological insulators or superconductors).

## ACKNOWLEDGMENTS

The authors thank A. Weindl and C. Setescak for carefully proofreading the manuscript and are grateful to A. Donarini for many fruitful discussions. In addition, the authors acknowledge the German Research Foundation (SFB 1277, Project No. 314695032) for funding.

## DATA AVAILABILITY

The data that support the findings of this article are openly available [94].

[1] D. M. Eigler and E. K. Schweizer, Positioning single atoms with a scanning tunneling microscope, Nature (London) **344**, 524 (1990).
[2] J. A. Stroscio and R. J. Celotta, Controlling the dynamics of a single atom in lateral atom manipulation, Science **306**, 242 (2004).
[3] M. R. Slot, T. S. Gardenier, P. H. Jacobse, G. C. Van Miert, S. N. Kempkes, S. J. Zevenhuizen, C. M. Smith, D. Vanmaekelbergh, and I. Swart, Experimental realization and characterization of an electronic Lieb lattice, Nat. Phys. **13**, 672 (2017).
[4] R. Drost, T. Ojanen, A. Harju, and P. Liljeroth, Topological states in engineered atomic lattices, Nat. Phys. **13**, 668 (2017).
[5] K. K. Gomes, W. Mar, W. Ko, F. Guinea, and H. C. Manoharan, Designer Dirac fermions and topological phases in molecular graphene, Nature (London) **483**, 306 (2012).
[6] S. N. Kempkes, M. R. Slot, J. J. van den Broeke, P. Capiod, W. A. Benalcazar, D. Vanmaekelbergh, D. Bercioux, I. Swart, and C. Morais Smith, Robust zero-energy modes in an electronic higher-order topological insulator, Nat. Mater. **18**, 1292 (2019).
[7] S. N. Kempkes, P. Capiod, S. Ismaili, J. Mulkens, L. Eek, I. Swart, and C. Morais Smith, Compact localized boundary states in a quasi-1D electronic diamond-necklace chain, Quantum Front. **2**, 1 (2023).
[8] S. E. Freeney, J. J. van den Broeke, A. J. J. Harsveld van der Veen, I. Swart, and C. Morais Smith, Edge-dependent topology in Kekulé lattices, Phys. Rev. Lett. **124**, 236404 (2020).
[9] C. F. Hirjibehedin, C. P. Lutz, and A. J. Heinrich, Spin coupling in engineered atomic structures, Science **312**, 1021 (2006).
[10] D. Serrate, P. Ferriani, Y. Yoshida, S.-W. Hla, M. Menzel, K. von Bergmann, S. Heinze, A. Kubetzka, and R. Wiesendanger, Imaging and manipulating the spin direction of individual atoms, Nat. Nanotechnol. **5**, 350 (2010).
[11] T. Esat, D. Borodin, J. Oh, A. J. Heinrich, F. S. Tautz, Y. Bae, and R. Temirov, A quantum sensor for atomic-scale electric and magnetic fields, Nat. Nanotechnol. **19**, 1466 (2024).
[12] A. J. Heinrich, C. P. Lutz, J. A. Gupta, and D. M. Eigler, Molecule cascades, Science **298**, 1381 (2002).
[13] A. A. Khajetoorians, J. Wiebe, B. Chilian, and R. Wiesendanger, Realizing all-spin–based logic operations atom by atom, Science **332**, 1062 (2011).
[14] C. R. Moon, L. S. Mattos, B. K. Foster, G. Zeltzer, and H. C. Manoharan, Quantum holographic encoding in a two-dimensional electron gas, Nat. Nanotechnol. **4**, 167 (2009).
[15] F. E. Kalff, M. P. Rebergen, E. Fahrenfort, J. Girovsky, R. Toskovic, J. L. Lado, J. Fernández-Rossier, and A. F. Otte, A kilobyte rewritable atomic memory, Nat. Nanotechnol. **11**, 926 (2016).
[16] S. Crampin, Scanning tunneling spectroscopy of surfaces where surface states dominate, J. Electron Spectrosc. Relat. Phenom. **109**, 51 (2000).
[17] L. Schneider, K. T. Ton, I. Ioannidis, J. Neuhaus-Steinmetz, T. Posske, R. Wiesendanger, and J. Wiebe, Proximity superconductivity in atom-by-atom crafted quantum dots, Nature (London) **621**, 60 (2023).
[18] M. Weiss, M. Schelchshorn, F. Stilp, A. J. Weymouth, and F. J. Giessibl, Increasing the lifetime of confined electronic states in an artificial quantum structure, Phys. Rev. B **109**, 235422 (2024).
[19] M. F. Crommie, C. P. Lutz, and D. M. Eigler, Confinement of electrons to quantum corrals on a metal surface, Science **262**, 218 (1993).
[20] M. A. Kastner, Artificial atoms, Phys. Today **46**(1), 24 (1993).
[21] F. Stilp, A. Bereczuk, J. Berwanger, N. Mundigl, K. Richter, and F. J. Giessibl, Very weak bonds to artificial atoms formed by quantum corrals, Science **372**, 1196 (2021).
[22] E. Sierda, X. Huang, D. I. Badrtdinov, B. Kiraly, E. J. Knol, G. C. Groenenboom, M. I. Katsnelson, D. Wegner, and A. A. Khajetoorians, Quantum simulator to emulate lower-dimensional molecular structure, Science **380**, 1048 (2023).
[23] W. Jolie, T. C. Hung, L. Niggli, B. Verlhac, N. Hauptmann, D. Wegner, and A. A. Khajetoorians, Creating tunable quantum corrals on a Rashba surface alloy, ACS Nano **16**, 4876 (2022).
[24] M. Chen, Y.-P. Jiang, J. Peng, H. Zhang, C.-Z. Chang, X. Feng, Z. Fu, F. Zheng, P. Zhang, L. Wang, K. He, X.-C. Ma, and Q.-K. Xue, Selective trapping of hexagonally warped topological surface states in a triangular quantum corral, Sci. Adv. **5**, eaaw3988 (2019).
[25] C. L. Degen, F. Reinhard, and P. Cappellaro, Quantum sensing, Rev. Mod. Phys. **89**, 035002 (2017).
[26] A. J. Heinrich, W. D. Oliver, L. M. K. Vandersypen, A. Ardavan, R. Sessoli, D. Loss, A. B. Jayich, J. Fernandez-Rossier, A. Laucht, and A. Morello, Quantum-coherent nanoscience, Nat. Nanotechnol. **16**, 1318 (2021).
[27] D. P. DiVincenzo, The physical implementation of quantum computation, Fortschr. Phys. **48**, 771 (2000).
[28] J. P. Dowling and G. J. Milburn, Quantum technology: The second quantum revolution, Phil. Trans. R. Soc. A **361**, 1655 (2003).
[29] T. Hayashi, T. Fujisawa, H. D. Cheong, Y. H. Jeong, and Y. Hirayama, Coherent manipulation of electronic states in a double quantum dot, Phys. Rev. Lett. **91**, 226804 (2003).
[30] C. P. Williams, *Explorations in Quantum Computing* (Springer, London, 2010).
[31] K. Yang, W. Paul, S.-H. Phark, P. Willke, Y. Bae, T. Choi, T. Esat, A. Ardavan, A. J. Heinrich, and C. P. Lutz, Coherent spin

manipulation of individual atoms on a surface, Science **366**, 509 (2019).

[32] See Supplemental Material at http://link.aps.org/supplemental/10.1103/2bsk-8cvx for the experimental details (SM1), a description of the construction plans of the investigated corrals (SM2), the model description of the quantum corral (SM3), details about the used filtering (SM4), a description of the multiple scattering simulations (SM5), the evaluation of the tip induced change in the total surface charge density (SM6), the definition of the frequency shift contrast and the error bars (SM7), the analysis of a second measurement set in a second corral (SM8), an estimate of the lateral CO bending during scanning (SM9), more details about the model descriptions of repulsion and attraction (SM10), the correction to the fitted attractive decay length in a Morse-type potential (SM11), and which includes Refs. [33–39].

[33] F. J. Giessibl, High-speed force sensor for force microscopy and profilometry utilizing a quartz tuning fork, Appl. Phys. Lett. **73**, 3956 (1998).

[34] T. R. Albrecht, P. Grütter, D. Horne, and D. Rugar, Frequency modulation detection using high-Q cantilevers for enhanced force microscope sensitivity, J. Appl. Phys. **69**, 668 (1991).

[35] M. Emmrich, F. Huber, F. Pielmeier, J. Welker, T. Hofmann, M. Schneiderbauer, D. Meuer, S. Polesya, S. Mankovsky, D. Ködderitzsch, H. Ebert, and F. J. Giessibl, Subatomic resolution force microscopy reveals internal structure and adsorption sites of small iron clusters, Science **348**, 308 (2015).

[36] J. Welker and F. J. Giessibl, Revealing the angular symmetry of chemical bonds by atomic force microscopy, Science **336**, 444 (2012).

[37] J. Welker, A. J. Weymouth, and F. J. Giessibl, The influence of chemical bonding configuration on atomic identification by force spectroscopy, ACS Nano **7**, 7377 (2013).

[38] P. Wahl, L. Diekhöner, M. A. Schneider, and K. Kern, Background removal in scanning tunneling spectroscopy of single atoms and molecules on metal surfaces, Rev. Sci. Instrum. **79**, 043104 (2008).

[39] A. J. Weymouth, T. Hofmann, and F. J. Giessibl, Quantifying molecular stiffness and interaction with lateral force microscopy, Science **343**, 1120 (2014).

[40] W. Shockley, On the surface states associated with a periodic potential, Phys. Rev. **56**, 317 (1939).

[41] M. Schneiderbauer, M. Emmrich, A. J. Weymouth, and F. J. Giessibl, CO tip functionalization inverts atomic force microscopy contrast via short-range electrostatic forces, Phys. Rev. Lett. **112**, 166102 (2014).

[42] F. J. Giessibl, A direct method to calculate tip–sample forces from frequency shifts in frequency-modulation atomic force microscopy, Appl. Phys. Lett. **78**, 123 (2001).

[43] B. Schuler, W. Liu, A. Tkatchenko, N. Moll, G. Meyer, A. Mistry, D. Fox, and L. Gross, Adsorption geometry determination of single molecules by atomic force microscopy, Phys. Rev. Lett. **111**, 106103 (2013).

[44] E. J. Heller, M. F. Crommie, C. P. Lutz, and D. M. Eigler, Scattering and absorption of surface electron waves in quantum corrals, Nature (London) **369**, 464 (1994).

[45] M. F. Crommie, C. P. Lutz, and D. M. Eigler, Imaging standing waves in a two-dimensional electron gas, Nature (London) **363**, 524 (1993).

[46] P. O. Gartland and B. J. Slagsvold, Transitions conserving parallel momentum in photoemission from the (111) face of copper, Phys. Rev. B **12**, 4047 (1975).

[47] R. Courths, M. Lau, T. Scheunemann, H. Gollisch, and R. Feder, From the Shockley surface state on Cu(111) to sp-like surface resonances on $Cu_3Au$(111), Phys. Rev. B **63**, 195110 (2001).

[48] F. Forster, G. Nicolay, F. Reinert, D. Ehm, S. Schmidt, and S. Hüfner, Surface and interface states on adsorbate covered noble metal surfaces, Surf. Sci. **532–535**, 160 (2003).

[49] P. Hyldgaard and T. L. Einstein, Surface-state mediated three-adsorbate interaction: Electronic nature and nanoscale consequences, Surf. Sci. **532–535**, 600 (2003).

[50] G. Butti, S. Caravati, G. P. Brivio, M. I. Trioni, and H. Ishida, Image potential states and electronic structure of Na/Cu(111), Phys. Rev. B **72**, 125402 (2005).

[51] H. Bekhouche, D. Rahou, A. Gueddim, M. K. Abdelhafidi, and N. Bouarissa, Electron states, effective masses and transverse effective charge of InAs quantum dots, Opt. Quantum Electron. **50**, 309 (2018).

[52] S. E. Freeney, S. T. Borman, J. W. Harteveld, and I. Swart, Coupling quantum corrals to form artificial molecules, SciPost Phys. **9**, 085 (2020).

[53] F. J. Giessibl, The qPlus sensor, a powerful core for the atomic force microscope, Rev. Sci. Instrum. **90**, 011101 (2019).

[54] Although both measurement sets were performed on the same sample, multiple sputtering and annealing cycles were carried out between the two sessions. Furthermore, the mesoscopic configuration of the tip was different. During the interval between the two measurement runs, the tip apex was modified several hundred times through slight and controlled indentations into the copper sample.

[55] Y. S. Kim, S. K. Kim, and W. D. Lee, Dependence of the closed-shell repulsive interaction on the overlap of the electron densities, Chem. Phys. Lett. **80**, 574 (1981).

[56] N. Moll, L. Gross, F. Mohn, A. Curioni, and G. Meyer, A simple model of molecular imaging with noncontact atomic force microscopy, New J. Phys. **14**, 083023 (2012).

[57] M. Ellner, P. Pou, and R. Pérez, Molecular identification, bond order discrimination, and apparent intermolecular features in atomic force microscopy studied with a charge density based method, ACS Nano **13**, 786 (2019).

[58] A. Liebig, P. Hapala, A. J. Weymouth, and F. J. Giessibl, Quantifying the evolution of atomic interaction of a complex surface with a functionalized atomic force microscopy tip, Sci. Rep. **10**, 14104 (2020).

[59] J. C. Slater, Atomic shielding constants, Phys. Rev. **36**, 57 (1930).

[60] N. D. Lang, Apparent barrier height in scanning tunneling microscopy, Phys. Rev. B **37**, 10395 (1988).

[61] M. Ternes, C. González, C. P. Lutz, P. Hapala, F. J. Giessibl, P. Jelínek, and A. J. Heinrich, Interplay of conductance, force, and structural change in metallic point contacts, Phys. Rev. Lett. **106**, 016802 (2011).

[62] G. Baym, *Lectures on Quantum Mechanics* (W.A. Benjamin, New York, 1969).

[63] P. Jelínek, M. Ondráček, and F. Flores, Relation between the chemical force and the tunnelling current in atomic point

contacts: A simple model, J. Phys.: Condens. Matter **24**, 084001 (2012).

[64] S. Nordholm and G. B. Bacskay, The basics of covalent bonding in terms of energy and dynamics, Molecules **25**, 2667 (2020).

[65] A. Gustafsson, N. Okabayashi, A. Peronio, F. J. Giessibl, and M. Paulsson, Analysis of STM images with pure and co-functionalized tips: A first-principles and experimental study, Phys. Rev. B **96**, 085415 (2017).

[66] A. Bereczuk, Universal HOM-type S-matrix correlations in chaotic (non-)trivial topological insulators and an improved model for the AFM and STM characteristics in Cu-based quantum corrals, Ph.D. thesis, University of Regensburg, 2022.

[67] Equivalent to the calculation of the decay length of the quantum corral states, the tips decay length is approximated by $\lambda_{\mathrm{tip}} = \sqrt{\hbar^2/(2m_e(\Phi + 440\,\mathrm{meV})} = 84$ pm, where $m_e$ is the electron mass and $\Phi = 4.95$ eV the work function of copper. In this approximation, the decay length of the tip is calculated at the onset of the Shockley surface state, which is 440 meV below the Fermi level. Between the band edge of the Shockley surface state and the Fermi energy, $\lambda_{\mathrm{tip}}$ only varies by 5%. This variation is neglected here and will not change the interpretation.

[68] P. M. Morse, Diatomic molecules according to the wave mechanics. II. Vibrational levels, Phys. Rev. **34**, 57 (1929).

[69] A. Mirzanejad and S. A. Varganov, Derivation of Morse potential, Mol. Phys. **123**, e2360542 (2025).

[70] G. Rubio-Bollinger, P. Joyez, and N. Agraït, Metallic adhesion in atomic-size junctions, Phys. Rev. Lett. **93**, 116803 (2004).

[71] H. Inouye and S. Kita, Experimental determination of the repulsive potentials between K+ ions and rare-gas atoms, J. Chem. Phys. **56**, 4877 (1972).

[72] H. Inouye and S. Kita, Elastic scattering of Li+ ions in helium, J. Chem. Phys. **57**, 1301 (1972).

[73] H. Inouye and S. Kita, Experimental determination of repulsive potentials between alkali ions (Li+, K+, and Cs+) and hydrogen molecules ($H_2$ and $D_2$), J. Chem. Phys. **59**, 6656 (1973).

[74] S. Kita, K. Noda, and H. Inouye, Experimental determination of repulsive potentials between alkali ions (Li+, Na+, and K+) and $N_2$ and CO molecules, Chem. Phys. **7**, 156 (1975).

[75] S. Kita, K. Noda, and H. Inouye, Repulsive potentials for Cl-R and Br-R (R = He, Ne, and Ar) derived from beam experiments, J. Chem. Phys. **64**, 3446 (1976).

[76] H. Inouye, K. Noda, and S. Kita, Repulsive potentials derived from beam scattering of Rb+ and Cs+ ions by rare gas atoms, J. Chem. Phys. **71**, 2135 (1979).

[77] C. Nordling, E. Sokolowski, and K. Siegbahn, Precision method for obtaining absolute values of atomic binding energies, Phys. Rev. **105**, 1676 (1957).

[78] M. Li, J.-Y. Zhang, Y. Zhang, and T.-M. Wang, A density functional theory study on the adsorption of CO and $O_2$ on Cu-terminated $Cu_2O(111)$ surface, Chin. Phys. B **21**, 067302 (2012).

[79] S. Saini, J. Halldin Stenlid, and F. Abild-Pedersen, Electronic structure factors and the importance of adsorbate effects in chemisorption on surface alloys, npj Comput. Mater. **8**, 163 (2022).

[80] X. Wang, L. Andrews, S. Riedel, and M. Kaupp, Mercury is a transition metal: The first experimental evidence for $HgF_4$, Angew. Chem. Int. Ed. **46**, 8371 (2007).

[81] A. Y. Rogachev, M. Miao, G. Merino, and R. Hoffmann, Molecular $CsF_5$ and $CsF_2^+$, Angew. Chem. **127**, 8393 (2015).

[82] P. F. Walch and D. E. Ellis, Effects of secondary ligands on the electronic structure of uranyls, J. Chem. Phys. **65**, 2387 (1976).

[83] K. Tatsumi and R. Hoffmann, Bent cis $d^0$ $MoO_2^{2+}$ vs Linear trans $d^0f^0$ $UO_2^{2+}$: A significant role for nonvalence 6p orbitals in uranyl, Inorg. Chem. **19**, 2656 (1980).

[84] P. Pyykkö, N. Runeberg, M. Straka, and K. G. Dyall, Could uranium(XII)hexoxide, $UO_6$ ($O_h$) exist? Chem. Phys. Lett. **328**, 415 (2000).

[85] V. G. Orlov and G. S. Sergeev, Electronic band structure and chemical bonding in trigonal Se and Te, AIP Adv. **12**, 055110 (2022).

[86] J. Lee, D. Wong, J. Velasco, J. F. Rodriguez-Nieva, S. Kahn, H. Z. Tsai, T. Taniguchi, K. Watanabe, A. Zettl, F. Wang, L. S. Levitov, and M. F. Crommie, Imaging electrostatically confined Dirac fermions in graphene quantum dots, Nat. Phys. **12**, 1032 (2016).

[87] D. M. Eigler, C. P. Lutz, and W. E. Rudge, An atomic switch realized with the scanning tunnelling microscope, Nature (London) **352**, 600 (1991).

[88] B. Neu, G. Meyer, and K.-H. Rieder, Controlled vertical and lateral manipulation of single atoms and molecules with the scanning tunneling microscope, Mod. Phys. Lett. B **09**, 963 (1995).

[89] H. Mönig, D. R. Hermoso, O. Díaz Arado, M. Todorović, A. Timmer, S. Schüer, G. Langewisch, R. Pérez, and H. Fuchs, Submolecular imaging by noncontact atomic force microscopy with an oxygen atom rigidly connected to a metallic probe, ACS Nano **10**, 1201 (2016).

[90] H. Mönig, S. Amirjalayer, A. Timmer, Z. Hu, L. Liu, O. Díaz Arado, M. Cnudde, C. A. Strassert, W. Ji, M. Rohlfing, and H. Fuchs, Quantitative assessment of intermolecular interactions by atomic force microscopy imaging using copper oxide tips, Nat. Nanotechnol. **13**, 371 (2018).

[91] B. Verlhac, N. Bachellier, L. Garnier, M. Ormaza, P. Abufager, R. Robles, M. L. Bocquet, M. Ternes, N. Lorente, and L. Limot, Atomic-scale spin sensing with a single molecule at the apex of a scanning tunneling microscope, Science **366**, 623 (2019).

[92] R. Wiesendanger, H.-J. Güntherodt, G. Güntherodt, R. J. Gambino, and R. Ruf, Observation of vacuum tunneling of spin-polarized electrons with the scanning tunneling microscope, Phys. Rev. Lett. **65**, 247 (1990).

[93] M. Bode, Spin-polarized scanning tunnelling microscopy, Rep. Prog. Phys. **66**, 523 (2003).

[94] M. Weiss, F. Stilp, M. Reinhart, and F. J. Giessibl, "Datasets for manuscript: Measurement and qualitative explanation of decay lengths of attractive and repulsive forces between natural and artificial atoms (2025)", https://epub.uni-regensburg.de/77379/.